Blast Load Profiles Over a Surrogate Human Skull With and Without a Helmet: Computational Analysis of Shock Tube Experiments

J. Magallanes[1], N. Meisner[1], S. Fu[1], J. Hamilton[1], A. Nelson[2], and P. VandeVord[2]

[1]*Karagozian & Case, 500 N. Brand Blvd., Ste. 1500, Glendale, CA, U.S.A.*
magallanes@kcse.com
[2]*Virginia Tech Center for Injury Biomechanics, Blacksburg, VA*

Abstract. This paper describes an experimental and computational study focused on quantifying the blast pressure profile over a surrogate human skull with and without an Advanced Combat Helmet (ACH). Experiments are conducted using a large shock tube to measure incident and reflected pressure-time histories at discrete points directly on a surrogate human skull surface. The skull was oriented face-on towards the inbound incident wave inside the shock tube. Pressure histories predicted using a CFD model are shown first, alongside the measured pressure histories from the shock tube experiments, to evaluate the manipulation of the blast wave by the helmet, while investigating the efficacy of the CFD model to predict those loads. The CFD model predicts pressure-time histories consistent with shock tube experiments, including a pressure increase observed at the back of the skull with the ACH mounted to the skull. There is, however, very little impulse increase observed in both the shock tube and CFD results when accounting for the test replicate scatter. Then, predictions from both the CFD model and an empirical model, based on the Kingery-Bulmash model with simple modifications to account for clearing effects, are used to predict the pressure profiles around the skull and ACH for an HE charge in the free-field, as would commonly be of interest in blast protection applications. These comparisons indicate that the empirical blast methodology has the potential to provide conservative pressures and impulses around the surrogate skull with future investigation and refinements.

1. Introduction

Methods to quantify blast loads over a human body is of interest in many protection applications. The applications of primary relevance to this paper involve understanding blast wave interactions with humans, the resulting primary injury mechanisms, and analysis methods that can be used as tools to develop or evaluate the effectiveness of Personnel Protection Equipment (PPE). An incident blast wave generated by an energetic source, like a high explosive (HE) charge, will reflect off a human body and their PPE, generating a spatially and time- varying distribution of reflected, partially reflected, incident, and dynamic pressure around the surface of the body or PPE. The loading transmitted into the body, whether directly from these impending pressure waves, or as secondary load transfer paths through the PPE contacting the body, is complex and governs the actual pressure transmission into the organs of the body. After all, it is this pressure transmission that causes primary blast injuries, whether they manifest as tympanic membrane rupture (TMR, a.k.a. ear drum rupture), traumatic brain injuries (TBI or mild TBI), lung injuries, or any other injury of concern in airblast environments. PPE needs to be designed or qualified to provide the desired level of protection against these loading mechanisms to be effective.

This paper is specifically focused on quantifying the blast pressure profile over a surrogate human skull and use of analysis tools to assess the effectiveness of a helmet to shield the head from the blast loads. This is done through the experimental and computational study described in this paper. Though there are many previous studies that evaluate the effectiveness of helmets against incident blast waves or seek to standardize their testing and evaluation (e.g., [1] [2]), this study focuses instead on quantifying the spatial and temporal variations of the loads over the human head through both experiments and analysis models. Having validated analysis models, like those explored in the study, offer means to predict loads under many more conditions than can be feasibly tested, which offers great value in the design and evaluation of effectiveness of PPE like helmets, in addition to interpreting trends observable from the extant datasets. This is done experimentally using a large shock tube to measure incident and reflected pressure-time histories at discrete points directly on a surrogate human skull surface. Measurements of the incident blast wave generated in the shock tube were obtained using incident pressure gages mounted on the shock tube walls, which when combined with the pressure sensors mounted on the skull, provide data that quantifies the actual reflected pressures generated over the surface of the skull. Measurements were taken with and without an Advanced Combat Helmet (ACH), which provide metrics to assess the effectiveness of the ACH to shield the protected side of the skull from those pressures. The forces transmitted through the helmet back into the skull, however, was outside the scope of the present effort and may be the subject of a future effort.

The analysis methods evaluated for the study focus on an empirical methodology widely used in the blast-resistant design of structures, on one end of complexity, to a much more resolved and physics-

https://doi.org/10.52202/081621-0015

based Computational Fluid Dynamics (CFD) method on the other end. The empirical methodology is based on the Kingery-Bulmash model [3] for HE charges, where the angle of incidence and clearing effects are accounted for in a method we call KB++ in this paper. This method can be reproduced from blast effects manuals available in the open literature [4]. For the CFD model, we utilize the ArunaCFD solver [5], which solves the fully compressible form of the Euler equations. CFD methods, like those described in the paper, are now more widely available and validated for predicting blast loads from HE.

The study is described and reported in several concise sections, starting with a description of the methods used for both the experiments and analysis in Section 2. Section 3 presents both the experimental and analytic results. Pressure histories predicted using the CFD model are shown first, alongside the measured pressure histories from the shock tube experiments. They are presented for the bare skull (B-Sk) and the bare skull with the helmet (Sk+H) to evaluate the manipulation of the blast wave by the helmet, while investigating the efficacy of the CFD model to predict those loads. This establishes the validity of the CFD methodology against experiments. Then, predictions from both the empirical model (KB++) and the CFD model (ArunaCFD) are used to predict the pressure profiles around the skull and PPE for a HE charge in the free-field, as would commonly occur in many blast protection problems of interest. A HE charge of one pound (0.454 kg) of TNT (trinitrotoluene) is selected at a range of 5 feet (1.524 meters), for a scaled range of 5 ft/lbs$^{1/3}$ (1.983 m/kg$^{1/3}$) for the study. This scaled range is well within the range of applicability of the KB++ methodology, as well as for the CFD model. We focus on quantifying the efficacy of the empirical model with respect to the CFD model to evaluate if a fast-running empirical methodology can provide design loads from which to design or evaluate PPE. A brief discussion of the results is provided in Section 4, which is then followed by conclusions in Section 5.

2. Methods

2.1 Experiments

A large Advanced Blast Simulator (ABS) at Virginia Tech was used for the experiments, which is reported in detail in other references [6] and journal paper in preparation. The ABS, shown in Figure 1, consists of three sections: a pressure driver, the test section, and an end-wave eliminator. The test section has a 4 x 4 ft (1.22 x 1.22 m) test section, is 45 feet (13.7 m) long, and supports mounting cadavers or other physical surrogates like the skull used in this effort (Figure 1). The driver is a gas detonation system, which can generate peak pressures up to 70 psi (480 kPa) with up to 4 msec durations. For this effort, the incident pressure generated is 24 psi (170 kPa) with a 3 msec duration for this effort (40 psi-msec or 276 kPa-msec impulse), which was measured by incident gages mounted inside the shock tube. High-speed cameras recorded the test specimen through an observation window.

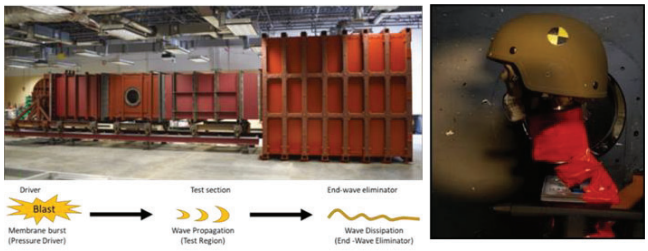

Figure 1. Experiment fixtures showing (left) the shock tube (ABS4 at Virginia Tech) and (right) instrumented surrogate human skull inside the test section stand with an ACH fixed to it.

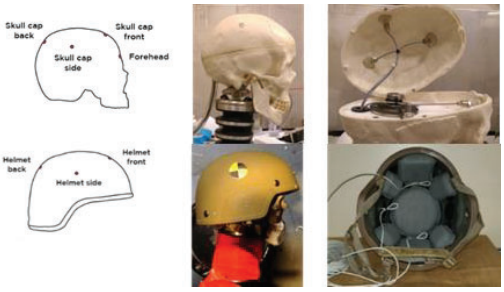

Figure 2. Pressure sensors mounted (top) on the skull and (bottom) on the helmet.

The test specimen is a synthetic human skull model (3B Scientific, Model 1020159) that was mechanically attached to a Hybrid-III neck-spine (Humanetics, Farmington Hills, MI) and secured to a test stand located mid-height of the shock tube section. The version secured with an ACH is shown in Figure 1 and can be configured in various orientations. The 0° face-on condition shown in Figure 1 is the focus in this paper. To capture pressure wave interactions within the helmet and skull, pressure sensors (Endevco, Model 8540-200) were placed on the test specimen as shown in Figure 2. For the skull, intracranial sensors were installed flush at the various locations shown in Figure 2. These

https://doi.org/10.52202/081621-0015

sensors were carefully selected and placed to measure the pressure in the air between the skull and the helmet while not interfering with the pads of the helmet. Additional sensors were placed on the helmet per Figure 2. Casting resin was poured into the skull to bond the neck bracket and seal off ocular and nasal passages.

2.2 CFD Methods

2.2.1 CFD Model and Solver

ArunaCFD is a compressible gas dynamics finite-volume solver for structured grids. The compressible gas dynamics are treated by solving the multi-species form of Euler's equations in three dimensions. The inviscid form of Euler's equations is solved using the piecewise parabolic method (PPM) for gases [7]. The PPM scheme employed in ArunaCFD is a high-order, finite-volume, monotonic upwind scheme for conservation laws (MUSCL), which is an example of a reconstruct-solve-average (RSA) method. ArunaCFD supports several Equations of State (EOS) for gases, including the ideal gas law leveraged to model air and the compressed gas inside of the shock tube.

In conservation form, these equations can be written as

$$\frac{\partial \rho}{\partial t} + \nabla \cdot \left(\rho v \right) \tag{1}$$

$$\frac{\partial \rho v}{\partial t} + \nabla \cdot \left(\rho v v + pI \right) = f_b \tag{2}$$

$$\frac{\partial \rho E}{\partial t} + \nabla \cdot \left(v \left[\rho E + p \right] \right) = \rho v \cdot f_b + \rho \dot{q}_c \tag{3}$$

$$\frac{\partial \rho X_i}{\partial t} + \nabla \cdot \left(\rho X_i v \right) = \dot{X}_i^c \tag{4}$$

where ρ is the density, v is the velocity vector, p is the pressure, X_i is the mass fraction of species *i*, $\dot{X}_i^c$ is the creation (or destruction) rate of species *i* due to any chemical or nuclear reactions present in the flow field, *E* is the sum of the internal ϵ and kinetic energy per unit mass,

$$E = \epsilon + \frac{1}{2}|v|^2 \tag{5}$$

$\dot{q}_c$ is the net (specific) energy deposition rate due to all reaction processes, f_b is the body force vector, and *t* is the time coordinate. Constraints on the mass fractions are imposed to enforce conservation of mass ($1 = \sum X_i$).

Finally, the EOS relating pressure to the internal energy, density, and composition closes this equation set,

$$p = p\left(\rho, \epsilon, X_i \right) \tag{6}$$

To treat high explosive (HE) detonation products, the Jones-Wilkins-Lee (JWL) EOS is used [8]. The form of the JWL implemented in ArunaCFD is written as follows:

$$p = A\left(1 - \frac{\omega}{R_1 V} \right) e^{-R_1 V} + B\left(1 - \frac{\omega}{R_2 V} \right) e^{-R_2 V} + \frac{\omega E}{V} \tag{7}$$

where *V* is the volume relative to the undetonated state (υ/υ_0). The parameters *A*, *B*, R_1, and R_2 are constant fitting parameters associated with the model, while ω is assumed-constant material parameter. *E* is the current internal energy per unit initial volume (e/υ_0).

Embedding complex surfaces in the CFD grid, like the skull and helmet, is accomplished using Immersed Boundary Methods (IBM) by reading faceted CAD geometry to modify the CFD grid values. The general idea with IBM is to place a complex geometry into a cartesian grid by modifying the cell values to conform to the surfaces describing the faceted geometry. The IBM is accomplished in ArunaCFD using the staircase methodology outlined by Ning et al.[9], which marks cell centers of the CFD mesh as stationary solids if they are within the boundaries of the input STL file. All other cells are treated as fluid under the gas dynamic laws described above. Any solid/gas interface in ArunaCFD is treated as reflective boundaries (slip) in ArunaCFD. The staircase methodology is binary, and results in either filled solid cells, or filled fluid cells. This may result in decreased accuracy near the boundary if grid cells are not refined enough to represent a complex surface.

https://doi.org/10.52202/081621-0015

2.2.2 Initial Conditions for Shock Tube Experiments

The CFD domain was set up to represent conditions inside the test chamber. The fixed grid, shown in Figure 3, measures 265 x 50 x 50 cm and is discretized with a resolution of 2 mm in each direction (approximately 8.5 M CFD grid cells). The dimension of the CFD were determined as a reduced model of the larger ABS shock tube. This "scaled" model is used for the computational domain, rather than modeling the exact dimensions of the ABS, to reduce the computational cost associated with the simulations. The boundary conditions included reflective conditions on the sides of the domain, reflective conditions on the driver side, and outflow conditions on the end-wave side (refer to Figure 1 for nomenclature). The air in the chamber was treated using the ideal gas law, while the driving side was initiated with a high energy gas using the same ideal gas law. The ideal gas properties of the high energy gas are computed by modifying the initial energy and temperature of the ideas gas to obtain a comparable pressure wave produced in the ABS. Computations were defined to run to 5 ms, which ran on 64 CPUs (Intel Xeon 5218, 2.3GHz, 32 CPUs, 256 GB DDR4 3200 RAM) using ArunaCFD's domain decomposition scheme leveraging the Message Passing Interface (MPI).

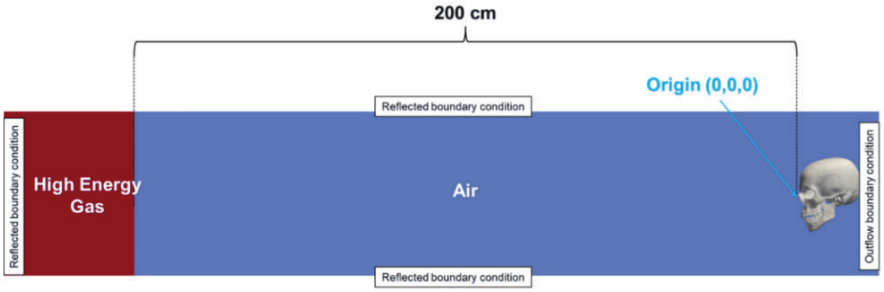

Figure 3. CFD model for the shock tube experiments.

Figure 4. IBM representations in the CFD model for the (a) B-Sk and (b) Sk+H cases.

The skull and ACH were inserted into the CFD domain using the IBM described earlier using faceted data obtained using actual laser scans of the test articles. Both versions of the skull with and without the ACH are shown in Figure 4. The leftmost part of each version shows the laser-scanned point cloud generated for the actual bare skull (a) or skull + helmet (b), the centermost shows the facetized data generated from the laser-scan data to create the STL file, and the rightmost shows the realization of the skull/ACH in the CFD grid.

2.2.3 Initial Conditions for Bare Explosives

A similar grid is used for the bare explosive simulation, which is shown in Figure 5. This fixed grid also measured 265 x 50 x 50 cm and is discretized with the same resolution 2 mm in each direction (approximately 8.5M CFD grid cells). The boundary conditions are defined as all outflow to model a free

https://doi.org/10.52202/081621-0015

field. As in the previous model, the air is treated using the same ideal gas law EOS, while the HE is treated using the JWL EOS with parameters calibrated for TNT. The one pound of TNT was modeled as a sphere having a diameter of 4 cm, which was determined using the density of TNT (1.63 g/cc).

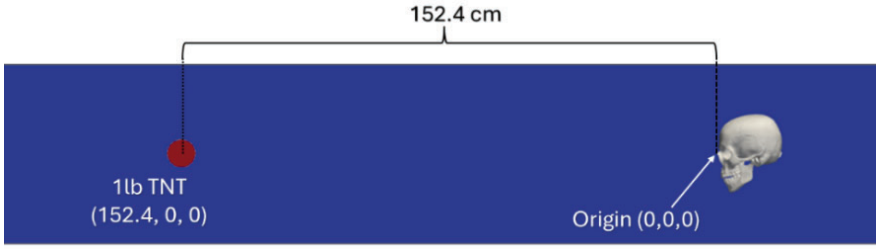

Figure 5. CFD model for the free air HE burst.

2.3 Empirical Methods

2.3.1 Kingery-Bulmash (K-B) Empirical Model

The K-B curves [3] are widely used to estimate blast loads on structures for spherical idealized free-air and hemispherical surface HE bursts [4], including those for finite-sized reflecting surfaces. They involve estimating blast wave parameters on those reflecting surfaces, including the peak reflected pressure and impulse (p_r, i_r), incident (or side-on) pressure and impulse (p_{so}, i_{so}), time of arrivals (t_{TOA}), as well as others that characterize the negative phase, all as a function of the scaled distance $Z=R/W^{1/3}$ (where R is the standoff distance and W is the equivalent weight of TNT). The method accounts for the effects of the angle of incidence (α) on the peak reflected pressure (p_{ra}) and the reflected impulse (i_{ra}), which then allows constructing pressure-time histories at any point of the reflecting surface [4].

Clearing effects are recognized in the methods to account for the reduction in total impulse that will occur at a point on a finite sized reflecting surface as compared with one having infinite size. In such cases, rarefaction waves, or clearing waves, will propagate from the edges of the reflecting surface towards the point of interest, relieving the inbound reflected wave. For finite-sized planar surfaces, like those on a building structure or component, the clearing time, t_c, is computed as:

$$t_c = \frac{4S}{(1+C_R)C_r} \tag{8}$$

where S is the smallest clearing distance, C_R is an aspect ratio parameter, and C_r is the sound velocity.

2.3.2 Application to obtain estimates of blast loads over the surrogate human skull and helmet

The KB++ procedures implement a very simple version of these methods to estimate loads on the skull and helmet. See Figure 6. First, the K-B blast wave parameters are computed in the normal way by calculating α for each point of interest (POI). For reflecting points (e.g., Pt. A in Figure 6(a)), the clearing time t_c is computed, as a first order approximation, as the distance to the closest point around the skull where α is 90 degrees (i.e., side-on). The methods described in the previous section are then used along with the assumption that clearing begins instantaneously[4]. Figure 6(b) shows the constructed pressure-time history. For non-reflecting points ($\alpha > 90$ degrees, like Pt. B in Figure 6(a)), side-on pressure is assumed with the distance computed according to the path illustrated that figure.

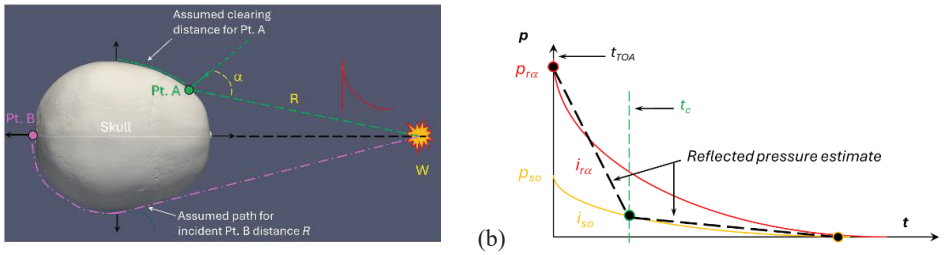

Figure 6. Schematic for KB++ pressure loads accounting for angle of incidence and clearing time.

https://doi.org/10.52202/081621-0015

3. Results

3.1 Shock Tube Experiments and CFD Comparisons

The CFD results match well against the experiments and exhibit both the reflected and diffraction waves expected over the skull and helmet. Static images showing pressure along a centerline plane of the CFD domain are shown in Figure 7, with the B-Sk case shown in Figure 7 and the Sk+H case shown in Figure 7. The case for Sk+H exhibits more complex reflections off the helmet, the most obvious ones in these figures being on the front side facing the blast.

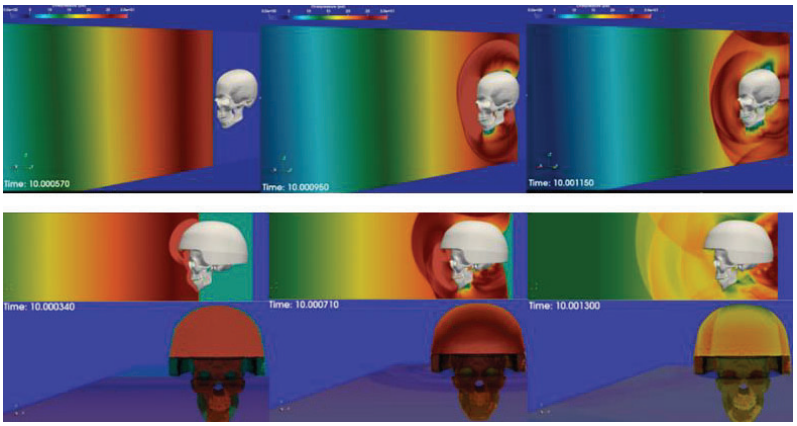

Figure 7. Pressures along the centerline of the shock tube CFD domain for the bare skull (Top: B-Sk) and the skull + helmet (Bottom: Sk+H). Note the snapshots are taken at different times in each simulation (msec).

The pressure histories measured at pressure gages shown on Figure 2(a) show very close alignment of the CFD results with the shock tube experiments. Figure 8 and Figure 9 plot pressure and impulse histories at the four gage locations on the skull for the B-Sk (Figure 8) and Sk+H (Figure 9): (a) Forehead, (b) Skull Cap Front, (c) Skull Cap Side, and (d) Skull Cap Back. Refer to Figure 2 for the illustration indicating their locations on the test articles. Shock tube data are plotted in black, which come from three replicate experiments, while the CFD results are plotted in blue. For the experimental data, one example pressure history is shown, while the envelope of impulses is shown from all three replicate experiments. However, this may result in some small discrepancies and differences between the CFD simulations and the experimental results. The One can observe that the pressure and impulse for the B-Sk case is highest at the Forehead, followed by the Skull Cap Front, Side, and Back, respectively. This behavior is observable from both the experimental and CFD results. One can also observe from the Sk+H case, that the helmet manipulates the pressure waves at the skull cap points under the helmet. The forehead traces, however, are virtually identical in both the B-Sk and Sk-H cases. It is worth noting that the CFD simulation is not an exact replica of the test facility shock tube, as modeling a 4ft x4ft x 45ft shock tube in a high-fidelity simulation would result in unacceptably long run times for the kind of analysis that is required. The CFD simulations here were configured in such a way as to reduce the overall length of the shock tube region while still maintaining consistent parameters that agreed with the initial conditions of the experiments.

Figure 10 presents this data in the form of bar plots for peak pressure (Figure 10(a)) and peak impulse (Figure 10(b)) measured at each of the skull pressure gages, with each plot (pressure (a) or impulse (b)) showing the B-Sk case on the left and the Sk+H on the right (including the three experimental replicates in each). It's worth noting here that the CFD initial conditions were configured against one specific test in the test series (Test 24a). The following plots show the comparison of the pressure profiles between both the CFD (orange), and the test series (blue) with the results from test 24a in dark blue, and the scatter of the test shown as transparent light blue. The helmet has an observable effect on the peak pressures, with the forehead and skull cap front experiencing the most significant drops, the skull cap side experiencing the least, while the skull cap rear conversely experiencing an increase, rather than a drop, in pressure. This trend is observed in both the CFD, and the experimental results. Total impulse, however, was relatively unchanged with or without the helmet, though the CFD results would imply some small drop in impulse across all the pressure gages with the helmet mounted on the skull.

https://doi.org/10.52202/081621-0015

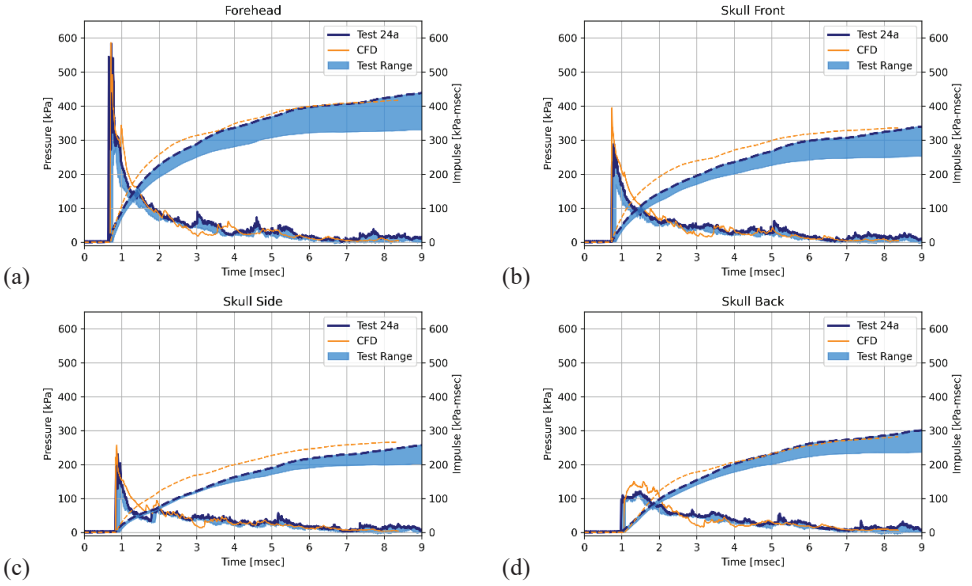

Figure 8. Shock tube CFD predictions versus experiments: Bare Skull (B-Sk).

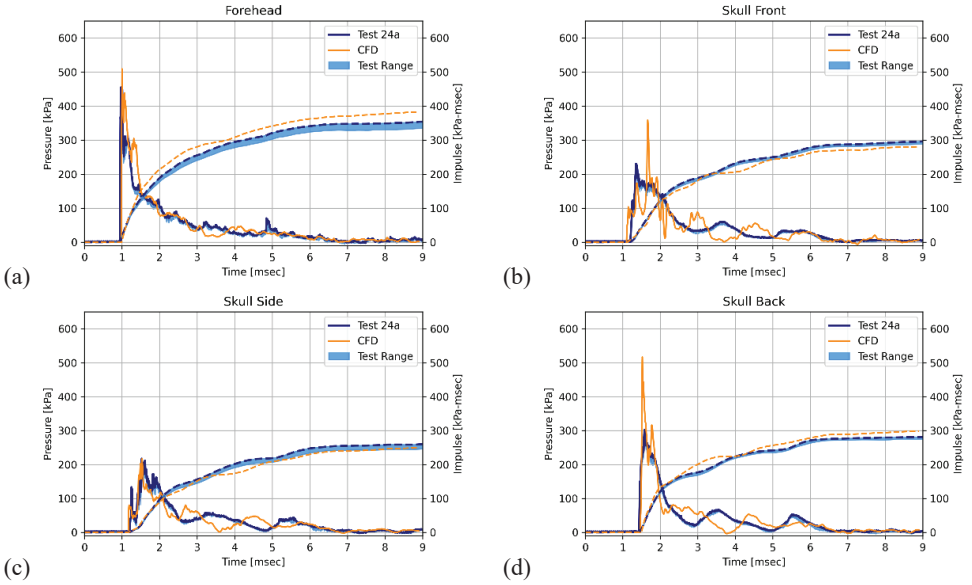

Figure 9. Shock tube CFD predictions versus experiments: Skull + Helmet (Sk+H).

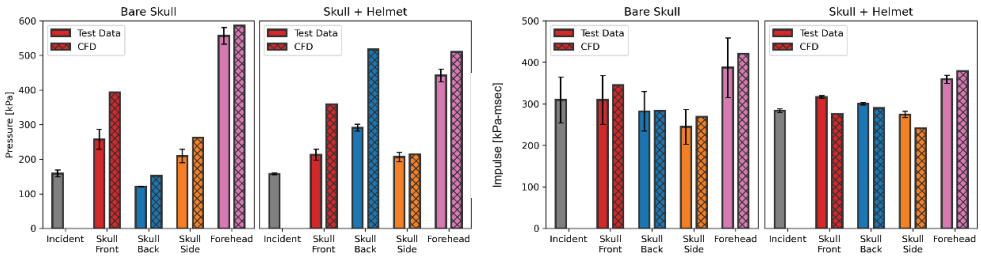

Figure 10. Comparison of peak pressure (a) and impulse (b) for the shock tube experiments and model.

https://doi.org/10.52202/081621-0015

Table 1. Summary of computed peak pressure and impulses for both the shock tube test series, and the CFD model. Pressures (p) are reported in kPa, while impulse is reported in kPa-msec.

St.	Bare Skull (B-Sk)						Skull + Helmet (Sk+H)					
	CFD		Test		%Difference		CFD		Test		%Difference	
	p	*i*	*p*	*i*	p_{diff}	i_{diff}	*p*	*i*	*p*	*i*	p_{diff}	i_{diff}
FH	578	415	579	431	0.2	3.7	510.0	386.0	553.0	351.0	7.8	10.0
SF	397	326	297	335	33.7	2.7	458.0	282.0	231.0	297.0	98.3	5.1
SS	268	261	233	252	15.0	3.6	229.0	240.0	229.0	256.0	0.0	6.3
SB	147	276	118	300	24.6	8.0	514.0	301.0	303.0	291.0	69.6	3.4
Average					18.4	4.5	**Average**				43.9	6.2

3.2 High-Explosive Pressure Distributions

Turning to the empirical KB++ model, which we intend to evaluate as a potential fast-running methodology for estimating pressures and impulses from HE charges, the studies for the same B-Sk and Sk+H cases show that under the one pound TNT charge (0.454 kg) at 5 feet of standoff (1.524 meters, Z=5 ft/lbs$^{1/3}$ (1.983 m/kg$^{1/3}$)), the KB++ methodology provides conservative pressure and impulse predictions, as compared with the CFD predictions

This is most effectively presented through the data shown in Figure 11, which shows computed pressure and impulse histories at four stations on the skull identified in Figure 12, and tabulated peak pressures and impulses presented in Table 1. These stations were selected slightly differently than in the shock tube experiments so that one can compare more reflected rather than side-on stations along the crown of the skull. Note from Figure 12, that Stations 1 and 3 have direct line-of-sight to the charge and would therefore experience reflected pressures proportional to, according to the K-B model, their angle of incidence (α), while Stations 4 and 6 are on the side and rear-face of the skull and would not reflect the inbound wave. Station 7, the rearmost station, was not selected because it is below and shielded by one of the ACH pads.

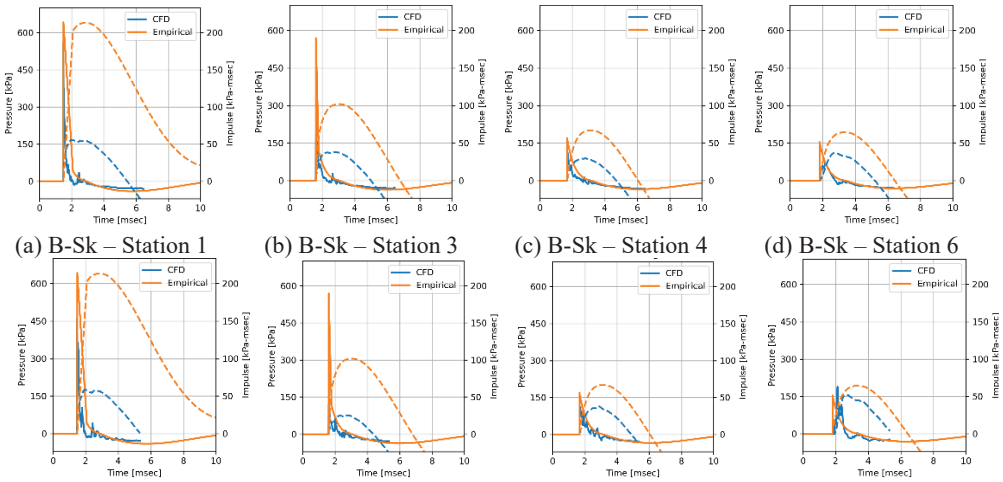

(a) B-Sk – Station 1 (b) B-Sk – Station 3 (c) B-Sk – Station 4 (d) B-Sk – Station 6

(e) Sk+H – Station 1 (f) Sk+H – Station 3 (g) Sk+H – Station 4 (h) Sk+H – Station 6

Figure 11. Calculated pressure histories at several stations designated in Figure 12 for the free-air HE burst of Z=5 ft/lbs$^{1/3}$ (1.983 m/kg$^{1/3}$) using the CFD and empirical (KB++) models.

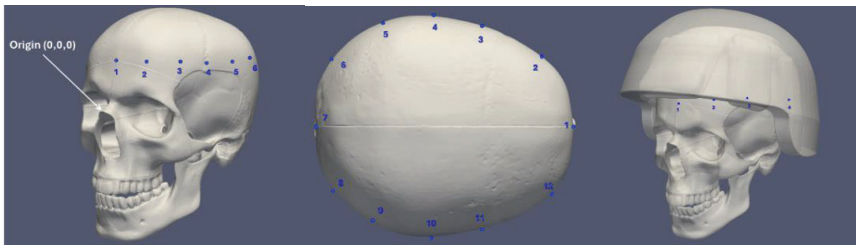

Figure 2. Stations selected along the crown of the skull for the empirical vs. CFD evaluation.

https://doi.org/10.52202/081621-0015

As can be seen in Figure 11 and Table 1, peak pressures and impulses are consistently higher than the CFD predictions for all Stations for both the B-Sk and Sk+H cases, except for Station 6 at the back of the skull for the SK+H case. For the B-Sk case, KB++ provides peak pressures and impulses that are 37.8% and 56.0% higher than the CFD predictions. For the Sk+H case, KB++ provides peak pressure and impulses that are 29.9% and 40.7% higher than the CFD predictions. On average, then, the KB++ methodology provide pressures and impulses that are higher and consistently more conservative than the CFD predictions. Station 6 is the only exception, on the other hand, where KB++ predicts a pressure less than the CFD prediction by 22.4%. This might indicate, when combined with the observations presented in the previous section concerning the shock tube data, that the KB++ methodology is missing any additional reflections in the helmet that might be contributing to the higher pressures observed consistently in the shock tube data at the back of the skull with the helmet in place (Sk+H). Refer to Figure 10 to evaluate these similarities; recall, that the helmet had appeared to amplify the peak pressure at gauge at the back of the skull, but that the total impulses were relatively unaffected by the presence of the helmet.

Table 2. Summary of computed peak pressure and impulses at Stations 1-7 for the free-air HE burst of Z=5 ft/lbs$^{1/3}$ (1.983 m/kg$^{1/3}$) using the CFD and empirical (KB++) models. Pressures (p) are reported in kPa, while impulse is reported in kPa-msec.

St.	Bare Skull (B-Sk)						Skull + Helmet (Sk+H)					
	CFD		Empirical		%Difference		CFD		Empirical		%Difference	
	p	i	p	i	p_{diff}	i_{diff}	p	i	p	i	p_{diff}	i_{diff}
1	559	55.6	642	213	12.9	74.0	461	58.4	642	213	28.2	72.6
2	284	33.7	610	145	53.4	76.8	280	35.8	610	145	54.0	75.3
3	273	38.3	569	102	52.0	62.5	168	25.6	569	102	70.5	74.9
4	130	29.7	169	66.9	23.4	55.7	111	37.9	169	66.9	34.2	43.3
5	92.2	30.7	161	65.6	42.8	53.2	N/A[1]	-	-	-	N/A[1]	N/A[1]
6	70.0	37.2	154	64.4	54.6	42.3	189	52.2	154	64.4	22.4	18.9
7	110	45.9	147	63.2	25.4	27.4	N/A[1]	-	-	-	N/A[1]	N/A[1]
Average					37.8	56.0	**Average**				29.9[2]	40.7

[1] - Station underneath helmet pad.
[2] - Average is calculated using absolute values.

4. Discussion

Investigation of the pressure fields (Figure 7(b)) present in the CFD model indicate, at least qualitatively, that these pressure rises occur from reflections generated by the incident wave interacting with the rear of the helmet. This might intuitively explain why there may be increases in reflected pressures at those rear-facing points, with very little increase, if any, on the total impulse imparted to the head. However, the complexity of the interactions of the incident, reflected, and diffractions waves around the skull and helmet makes it difficult to interpret. We have also only currently looked at the face-on orientation and would expect different orientations to display different distributions, at least on the rear-side of the skull.

Comparisons with the empirical equations and the CFD simulation show much larger average differences as compared to the average differences between the CFD and the shock tube in the previous section. Though there are many potentially explanations for this, we believe the primary one is likely due to the difficultly in predicting blast profiles over non-orthogonal surfaces using the empirical equations. Both the shock tube experiments and the CFD calculations appear to imply that geometric effects, and the complexity of the shockwaves generated around the skull are additional complexities that are not current accounted for the in the empirical equations. This is likely the cause of the better agreement of peak pressure at Station 1, which has the least geometric complexity. Additionally, the KB equations are empirically derived equations based on test data of bare high explosives. ArunaCFD uses an empirically derived equation of state (the JWL EOS), in which parameters for TNT are either gathered from test data, or thermochemical analysis tools. There are often errors association with these empirical fits for the equation of state for the CFD simulation which may be another reason there is larger discrepancies between the CFD and empirical equations, as compared to the CFD and the test data.

5. Summary and Conclusions

The experimental and computational results presented in this paper show that a CFD model predicts pressure-time histories consistent with shock tube experiments, and that an empirical blast

https://doi.org/10.52202/081621-0015

methodology, based on the K-B model called KB++, has the potential to provide conservative pressures and impulses around a surrogate skull for HE charges in the free-field with future investigation and refinements. The shock tube analysis was limited to an incident pressure wave of 24 psi and 40 psi-msec (t_d = 3 msec) but includes three replicate experiments, where the CFD results were within 34% and 8% of the pressure and impulse, respectively, and reproduced the distribution of the pressures and impulses measured in the experiments. The empirical methodology, which uses the K-B model by accounting for the angle-of-incidence and clearing time effects, in a very simple way, was shown to provide conservative pressure and impulses against the CFD from an HE charge in the free-field (Z=5 ft/lbs$^{1/3}$ (1.983 m/kg$^{1/3}$)), with exception the higher peak pressures observed at the back of the helmet, with empirical results within 34% and 48% of the pressure and impulse of CFD results, respectively. This study is, of course, limited to the shock tube conditions and HE scaled range evaluated in this study, and only in the face-on condition for the skull.

These efforts would benefit from extensions we are interested in pursuing in the future. First, the CFD analysis should be extended to experiments for different skull orientations. The face-on case evaluated here involves only a subset of conditions of interest to actual PPE applications (e.g.,[10]), and validation of the CFD model for other orientations would allow for applications in others that cannot be feasibly tested. Second, the KB++ methodology could likely be further extended to address the stated gaps and assumptions to provide fast-running conservative loads for purposes of designing and evaluating PPE. Though the KB++ method will not likely be a perfect substitute for either experiments or CFD analysis, it could certainly provide a quick design and analysis tool for evaluating effectiveness of PPE once refined and validated within known conditions. Finally, this experimental and analysis study was limited to the blast wave impinging on the skull and skull+helmet, which ignores the loads transferred through the helmet pads back into the skull. As we pointed eluded to in the introduction, this may be an important load transfer mechanism to consider for injury analysis and PPE design. Experiments and analysis tools that can provide insight into these load transfer mechanisms could allow for improved design of PPE.

References

[1] C. Carneal, A. Merkle, D. Zinn, J. Andrist, J. Clark, V. Alphonse, D. Ritzel, M. Carboni, B. DeCritofano and J. M. M. Cyganik, "Development of a Laboratory Shock Tube System for Helmet Blast Overpressure Performance Assessment," in *Proc. Personal Armour Systems Symposium (PASS) 2016*, Amsterdam, 2016.

[2] M. Maach, "Comparison of Hybrid III head response to shock tube and explosive blast loading," in *Int. Research Council on the Biomechanics of Injury (IRCOBI) Conf.*, Antwerp (Belgium), 2017.

[3] C. Kingery and G. Bulmash, "Airblast Parameters from TNT Spherical Air Burst and Hemispherical Surface Burst," U.S. Army Armament Research and Development Center, Ballistic Research Laboratory, Aberdeen Providing Ground, MD, 1984.

[4] Department of Defense, "Structures to Resist the Effects of Accidental Explosions, UFC-3-340-02," Whole Building Design Guide, http://dod.wbdg.org/, 2008.

[5] Karagaozian & Case, Inc., "ArunaCFD," [Online]. Available: https://www.kcse.com/arunacfd/. [Accessed 15 March 2025].

[6] A. Nelson, D. Ritzel, N. Showalter, D. Boppe, A. Riegel and P. VandeVord, "Characterization of an advanced blast simulator for investigation of lage scale blast traumatic brain injury studies," *Ann. Biomed. Eng.,* vol. 53, no. 1, pp. 133-142, 2024.

[7] P. Colella and P. Woodward, "The piecewise parabolic method (PPM) for gas-dynamical simulations.," *Journal of computational physics,* vol. 54, no. 1, pp. 174-201, 1984.

[8] E. L. Lee, H. C. Hornig and J. W. Kury, "Adiabatic expansion of high explosive detonation products," Lawrence Radiation Laboratory, University of California, Livermore, 1968.

[9] J. Ning, T. Ma and G. Lin, "A grid generator for 3-D explosion simulations using the staircase boundary approach in Cartesian coordinates based on STL models," *Adv. in Eng. Soft.,* vol. 67, pp. 148-155, 2014.

[10] D. Wallace and S. Rayner, "Combat Helmets and Blast Traumatic Brain Injury," *J. Mil. and Veterans Health,* vol. 20, no. 1, 2012.

https://doi.org/10.52202/081621-0015